Discover Applied Sciences

Research

Impact of transparent conducting substrates on structural and optical of Titanium(IV) phthalocyanine dichloride ($TiPcCl_2$) thin films

Sabrien M. Abdelhamid[1] · M. Dongol[1] · A. F. Elhady[1] · Amr Attia Abuelwafa[1]

Received: 1 August 2023 / Accepted: 20 November 2023
Published online: 30 January 2024

Abstract
This study investigates the impact of transparent conducting substrates, specifically indium-doped tin oxide (ITO) and fluorine-doped tin oxide (FTO), on the structural and optical characteristics of thermally evaporated Titanium phthalocyanine chloride ($TiPcCl_2$) thin films. The crystalline structure of $TiPcCl_2$/quartz thin films was verified by X-ray powder diffraction (XRD) patterns while amorphous phases were detected in $TiPcCl_2$/ITO and $TiPcCl_2$/FTO thin films. Field emission scanning electron microscopy (FESEM) images provided evidence that the morphology of $TiPcCl_2$ thin films may be affected by a lattice mismatch between $TiPcCl_2$ and substrates. Fourier-transform infrared spectroscopy (FT-IR) also showed that the substrates did not change the molecular structure of $TiPcCl_2$. UV–Vis-NIR spectroscopy demonstrated that the substrates had a significant influence on the optical gap, optical constants, dielectric constant dielectric loss functions and optical conductivity of $TiPcCl_2$ thin films. Lastly, the nonlinear susceptibility $\chi^{(3)}$, the nonlinear refractive index n_2 and the nonlinear absorption coefficient $\beta_{(c)}$ for $TiPcCl_2$/ITO, $TiPcCl_2$/FTO, and $TiPcCl_2$/quartz were obtained using a semi-empirical approach. The changes seen in optical properties could be due to changes in the crystal structure and morphology, which are closely connected to the properties of the substrate material. Overall, the results for $TiPcCl_2$ thin films are promising, and they are appropriate for novel optoelectronic device applications.

Article Highlights

- XRD, SEM, and FTIR spectra identified TiPcCl2 thin film crystal structure and morphology.
- The study examines how substrates affect the structural, linear, and nonlinear optical characteristics of $TiPcCl_2$.
- We estimated non-linear optical characteristics using an empirical relation.

Keywords $TiPcCl_2$ · Thin films · ITO · FTO · Linear and nonlinear optical

1 Introduction

Metal phthalocyanines (MPcs) have garnered significant interest in the field of organic electronics due to their exceptional performance, robust chemical and thermal stability, and cost-effectiveness [1, 2]. Derivatives of transition metals were synthesized. Moreover, there has been considerable interest in a number of MPcs compounds, which have been extensively

✉ Amr Attia Abuelwafa, amr.abuelwafa@sci.svu.edu.eg | [1]Nano and Thin Film Laboratory, Physics Department, Faculty of Science, South Valley University, Qena 83523, Egypt.

researched and widely acknowledged for their applicability in electronic device applications, including gas sensors, dye-sensitized solar cells, organic field-effect transistors, and others [1–6].

Titanium Phthalocyanine Chloride ($TiPcCl_2$) is a widely used derivative of metal phthalocyanines (MPcs), known for its exceptional stability and effective light absorption characteristics throughout the visible and near-infrared portions of the optical spectrum. Moreover, the compound has a conjugated system of 18π electrons. Additionally, $TiPcCl_2$ exhibits a p-type transport characteristic, hence enabling it to function as a semiconductor. Titanium Phthalocyanine Chloride ($TiPcCl_2$) is a widely used derivative of metal phthalocyanines (MPcs) that exhibits P-type mobilities, as reported in references [7–9]. Previous studies have mostly focused on investigating the influence of annealing temperature on the structure and features of $TiPcCl_2$ thin films. Additionally, the effects of film thickness and the coordinated ligand on the optical and electrical properties have also been extensively explored in the literature [7–9]. Nevertheless, there is a lack of prior research describing the impact of growth factors such as substrate temperature, doping condition, preparation technique, and substrate nature on the structural properties, as well as the linear and nonlinear optical properties of $TiPcCl_2$.

The type of substrate is regarded as one of the most critical elements influencing the structure, morphology, optical, and electrical characteristics of thin films. The significant impact of substrates on physical properties may be attributed to several variables, including substrate surface orientations, substrate surface conductivity, and lattice mismatch between thin films and substrates [10–16]. Therefore, it is important to consider the impact of substrates since they have a substantial influence on the physical characteristics of thin films. The linear optical characteristics of thin films may be influenced by the kind of substrate they are deposited on. An instance of this phenomenon is when a substrate with a high refractive index is used, resulting in an augmentation of the optical absorption of the thin film. This property may be advantageous in several applications that need light absorption, such as in the field of solar cell technology.

In recent studies, researchers have made efforts to create thin-film optical systems utilizing transparent conducting substrates (TCSs) like fluorine-doped tin oxide (FTO) coated glass and indium-doped tin oxide (ITO). This approach aims to capitalize on the advantageous characteristics of TCSs, such as their ability to abruptly terminate optical transmission in the near-infrared (NIR) range and their notable optical nonlinearities. The use of TCSs has significantly enhanced the process of light capture as well. The use of TCSs is possible with many optoelectronic devices owing to their distinctive properties. The use of TCSs has the potential to modify the nonlinear characteristics of organic materials such as CN-PPV/FTO [10], PTCDA/ITO [17] and NiTPP/FTO [18]. The investigation of the TCS substrate's impact on the linear and nonlinear optical characteristics of thin films is a necessary subsequent step, as shown by previous studies [10, 17, 18].

In general, the impact of the substrate on the structural properties and both linear and nonlinear optical behaviors of $TiPcCl_2$ when it is applied onto several transparent glass substrates, including ITO and FTO, represents a multifaceted and underexplored domain of investigation. Nevertheless, the existing early investigations indicate that the qualities in question may be substantially influenced by the substrate. Further investigation is required in order to fully comprehend the impact of the substrate on thin films of $TiPcCl_2$. The findings of this study have the potential to facilitate the advancement of novel and enhanced organic electronic gadgets using $TiPcCl_2$ as a fundamental component.

The objective of this study is to examine the alterations in the crystal structure of thin films of $TiPcCl_2$ resulting from the influence of transparent conducting substances. Additionally, this research aims to establish a connection between these structural modifications and the linear and nonlinear optical characteristics of the films. In order to achieve the objective, thin films of TiPcCl2 were fabricated through the thermal evaporation method on quartz, ITO, and FTO substrates under the same deposition conditions. The structural surface morphologies and molecular structure of these films were examined using XRD, FESEM, and FT-IR techniques, respectively. Additionally, the optical properties, including the optical band gap and optical constants, were determined by analyzing the transmittance T(λ) and reflectance R(λ) measurements at various wavelengths ranging from 200 to 2500 nm. Furthermore, we have calculated the non-linear optical parameters using a semi-empirical relation.

2 Experimental techniques

$TiPcCl_2$ powder was obtained from Sigma-Aldrich (see Scheme 1) and deposited at room temperature on clean ITO/glass FTO/glass, and quartz substrates by the thermal evaporation method (Edwards type E306A-10^{-6} Torr). The film thickness (250 nm) was measured using the crystal thickness monitor (FTM5). The XRD patterns for $TiPcCl_2$/TCSs were obtained using an XRD system (Rigaku RINT 2100 diffractometer). The surface properties of $TiPcCl_2$/TCSs films were studied using FESEM (QUANTA FEG250) and a transmission electron microscope (FESEM, JEOL model JSM-7001F). The chemical structure of the powder and TiPcCl2/TCSs films was examined using the Fourier transform infrared (FT-IR)

Scheme 1 Molecular structure of TiPcCl2

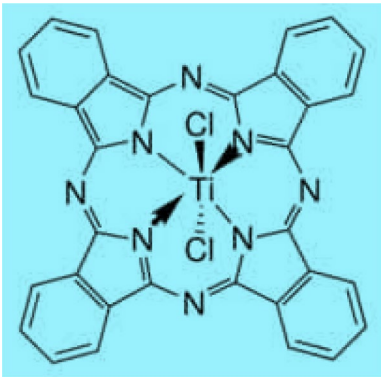

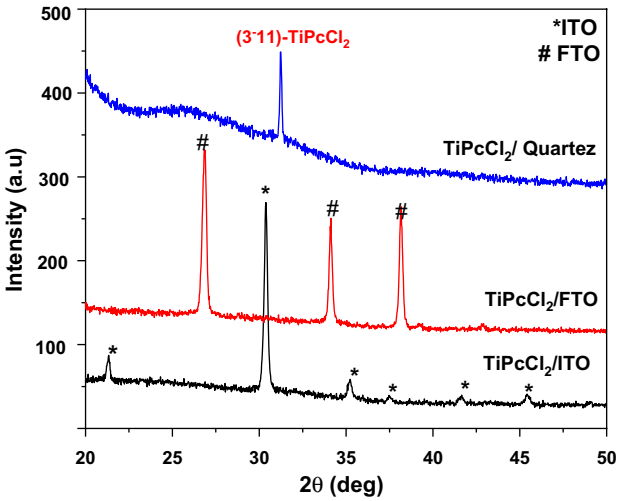

Fig. 1 XRD patterns of as deposited $TiPcCl_2$/quartz, $TiPcCl_2$/ITO and$TiPcCl_2$/FTO thin films

method (Jasco Model 6100) at room temperature in the spectral region 400–1600 cm^{-1}. The optical measurements were performed using a spectrophotometer (JASCO V-570) in the wavelength range of 200–2500 nm.

3 Result and discussion

3.1 Structural properties

The XRD patterns for $TiPcCl_2$ thin films are deposited onto ITO, FTO, and quartz substrates are shown in Fig. 1. From this figure, $TiPcCl_2$/ITO and $TiPcCl_2$/FTO thin films have an amorphous structure. There is no significant $TiPcCl_2$ peak in the case of ITO and FTO substrates, as they simply displayed the strong background peak of substrates. All of the peaks shown in these patterns are caused by ITO and FTO substrates. The amorphous phase in $TiPcCl_2$/ITO and $TiPcCl_2$/FTO thin films is caused by a lattice mismatch between $TiPcCl_2$ and the ITO and FTO substrates. The disparity in the lattice constants of two materials is known as a lattice mismatch. When the lattice mismatch is too great, the two materials cannot form a crystalline structure. Instead, the two materials will combine to produce an amorphous structure, which is a disordered structure with no long-range organization. However, $TiPcCl_2$/quartz has a predominantly single diffraction peak with preferred (-311) orientation and is centered at $2\theta = 31.17°$. This observation for TiPcCl2/quartz thin film is in agreement with results reported in the literature for the XRD pattern of TiPcCl2 in powder form [7]. Scherrer's equation [18, 19] is used to get the average crystallite size D. The nanostructure features of TiPcCl2/quartz thin film are confirmed by crystallite size values in the nanoscale (34 nm).

FESEM is an extremely useful instrument for comparing the surface morphology of thin films produced on various substrates. This data may be utilized to better understand how substrate type and deposition factors impact thin film

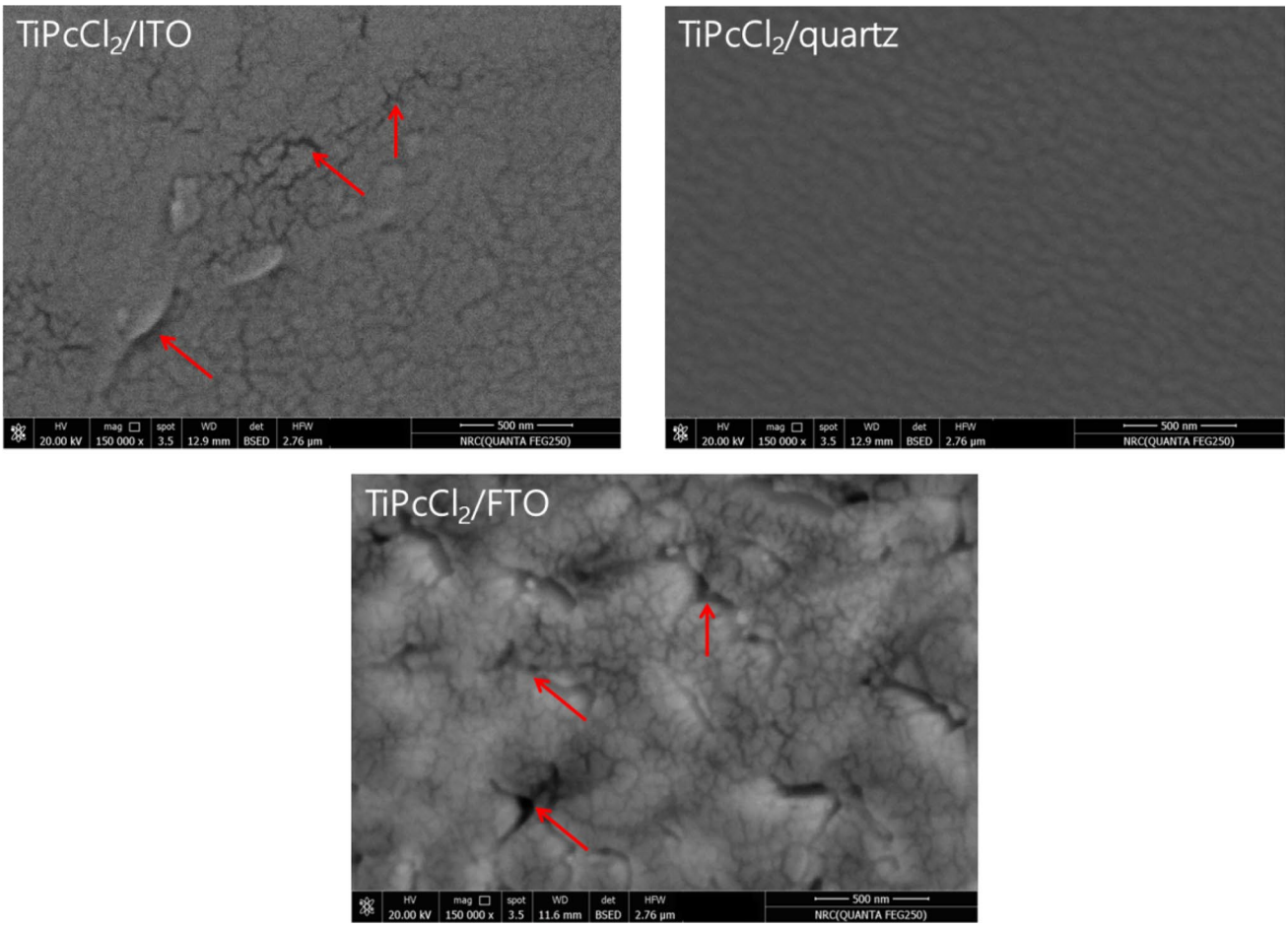

Fig. 2 FESEM for $TiPcCl_2$/FTO, $TiPcCl_2$/ITO, and $TiPcCl_2$/quartz thin films

nucleation and growth, as well as to optimize the deposition process to generate thin films with the required surface shape. Figure 2 shows FESEM images of $TiPcCl_2$/FTO, $TiPcCl_2$/ITO and $TiPcCl_2$/quartz thin films. It is obvious that the surfaces of $TiPcCl_2$/FTO and $TiPcCl_2$/ITO thin films exhibit non-smooth characteristics, displaying many voids and fractures in comparison to the $TiPcCl_2$/quartz thin film. The morphology of $TiPcCl_2$ thin films may be affected by lattice mismatch between $TiPcCl_2$ and substrates. A larger lattice mismatch might result in the creation of islands and other film defects. These flaws have the potential to impair the efficiency of solar cells and other electrical equipment.

Figure 3 displays the grain size distributions of $TiPcCl_2$/ITO, $TiPcCl_2$/FTO, and $TiPcCl_2$/quartz. The average grain sizes of $TiPcCl_2$ thin films deposited onto ITO, FTO, and quartz substrates are computed using Image J software and found to be around 100 ± 2, 68 ± 2, and 52 ± 2 nm, respectively. The analysis reveals that the average grain size values suggest that the produced films possess a nanostructured characteristic. The different grain sizes observed in $TiPcCl_2$ thin films on ITO, FTO, and quartz substrates might be related to the thermal expansion coefficients and lattice misfit between $TiPcCl_2$ and the substrates. Notably, the lattice mismatch is more evident in FTO than in ITO. This process enhanced the chance of fractures and cavities, resulting in grain fusion, higher grain sizes, and increased TiPcCl2 surface roughness on the FTO substrate [10, 11].

Furthermore, the observed grain size in the FESEM image of $TiPcCl_2$/quartz is much greater than the crystallite size estimated using XRD data of the corresponding films, as determined by Scherrer's equation. The grain size seen in the FESEM image may exhibit a larger value compared to the crystallite size determined using XRD analysis. In this study, it is postulated that the observed increase in crystallite size on the surface morphology of the film may be attributed to the aggregation of smaller crystals. Additionally, XRD analysis is used to determine the average crystallite size, which is indicative of the coherent scattering of X-rays [20, 21].

Analyzing infrared spectra of organic compounds is a widely used and efficient method for determining their molecular structures. Infrared spectra in the range 400–1600 cm^{-1} (fingerprint region) for $TiPcCl_2$ powder, $TiPcCl_2$/FTO, $TiPcCl_2$/

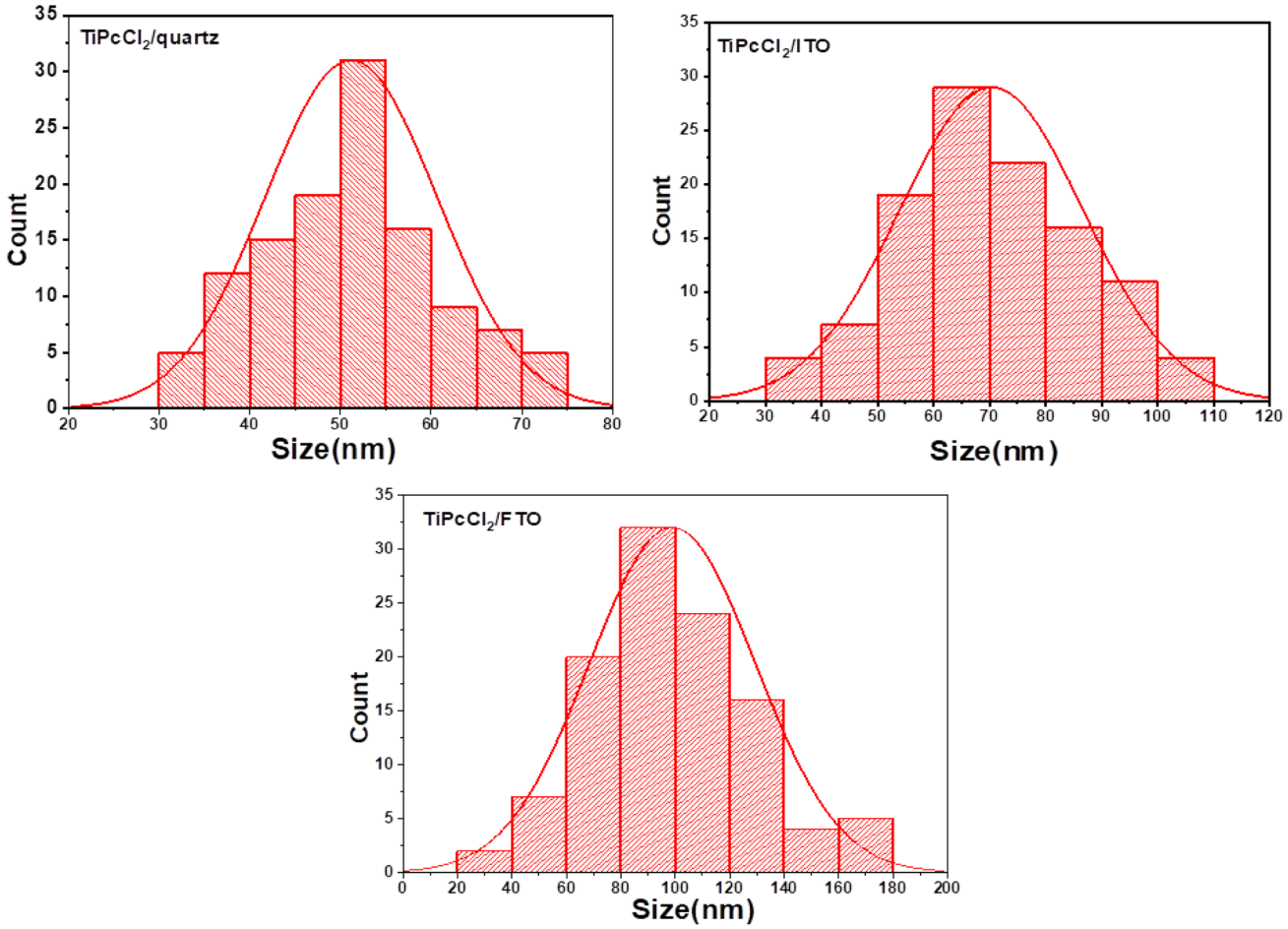

Fig. 3 Histogram of grain size distribution for $TiPcCl_2$/TCSs thin films

ITO, and $TiPcCl_2$/quartz thin films are shown in Fig. 4. Peak positions and assignments [22–24] are listed in Table 1. We noticed that the strength of the peaks reduced for compounds with varied substrates, indicating that the substrates had an influence on crystallization while keeping the chemical structure of the $TiPcCl_2$.

3.2 Optical characterization

The spectral distributions of T(λ) and R(λ) for $TiPcCl_2$/ITO, $TiPcCl_2$/FTO, and $TiPcCl_2$/quartz films over the wavelength range of 200–2000 nm are shown in (Figs. 5, 6). It is observed that at (λ > 1000 nm), transmittance values decline while reflectance values rise, owing to the free carriers in the ITO and FTO layers begin to absorb light, which reduces the transmittance and increases the reflectance. Also, the thickness of the ITO and FTO layers also affects the transmittance and reflectance of the films. A thicker ITO or FTO layer will absorb more light, which will reduce the transmittance and increase the reflectance. Furthermore, lower T (λ) and R (λ) for $TiPcCl_2$/ITO, $TiPcCl_2$/FTO, affirmed the increased scattering of photons with increasing crystal imperfections or structural disorder attributed to decreased crystallite size due to increased RMS roughness of the thin films [16]. Thus, structural alteration of the thin films on different glass substrates was responsible for the observed changes in transmittance and reflectance characteristics.

Using the following relationship we can determine the absorption coefficient (α) of $TiPcCl_2$/TCSs films from T (λ) and R (λ) measurements [25]:

$$\alpha = \frac{1}{d} ln\left(\frac{1-R^2}{2T} + \sqrt{R^2 + \frac{1-R^2}{4T^2}}\right) \quad (1)$$

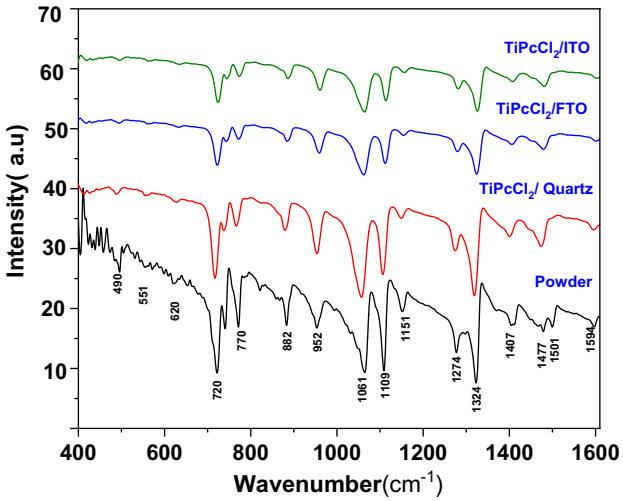

Fig. 4 FTIR spectra for $TiPcC_{l2}$ powder, $TiPcCl_2$/quartz and $TiPcCl_2$/TCSs

where *d* is the film thickness. The absorbance coefficient of the $TiPcCl_2$/FTO, $TiPcCl_2$/ITO, and $TiPcCl_2$/quartz thin films is depicted in Fig. 7. The spectrum displays three distinct bands. The Q band corresponds to the transition between the ground state and the first excited state ($S_0 \rightarrow S_1$). Q-band splitting can also be observed, while the Soret (B) band is associated with a strongly allowed transition from the ground state to the second excited state ($S_0 \rightarrow S_2$). The Q and Soret (B) bands are frequently associated with $\pi \rightarrow \pi^*$ singlet transitions [1, 2, 26–31]. In addition, a band called C occurs at 225 nm in the UV range due to the intrinsic transition of $TiPcCl_2$ ($n \rightarrow \pi^*$) [1, 2, 26–31]. Using Tauc's relation, the optical band gap can be determined in the strong absorption area (($\boldsymbol{\alpha} \geq 10^4\ cm^{-1}$)) [25]:

$$(\alpha h\nu)^m = H\left(h\nu - E_g^{opt}\right) \tag{2}$$

where H is a constant, E_g^{opt} is the optical band gap, and ***m*** is an index dependent on the type of electronic transition occurring in the substances. Considering the optimum match is gotten with $\boldsymbol{m=2}$, it is concluded that the electronic transition is an indirect permitted transition for $TiPcCl_2$/ITO, $TiPcCl_2$/FTO and $TiPcCl_2$/quartz thin films (Fig. 8). The first energy value E_{g1}^{Opt} corresponds to the optical absorption Q band, whereas the second energy value E_{g2}^{Opt} relates to the optical absorption B-band. The estimated values of the E_g^{Opt} of the $TiPcCl_2$/ITO, $TiPcCl_2$/FTO and $TiPcCl_2$/quartz thin films are listed in Table 2. Based on the findings presented in Fig. 8 and Table 2, it can be observed that the TiPcCl2/FTO film

Table 1 The Peak Positions and assignments for $TiPcCl_2$ powder, $TiPcCl_2$/quartz and $TiPcCl_2$/TCSs thin films

Powder (cm^{-1})	Thin films			Assignment
	$TiPcCl_2$/*quartz* (cm^{-1})	*TiPcCl*$_2$*/FTO* (cm^{-1})	$TiPcCl_2$/*ITO* (cm^{-1})	
1594	1595	1597	1598	*ν*(C–C) Benzene stretch
1475	1473	1478	1481	*β*(C–H) Aryle
1407	1406	1410	1413	ν(C–H) In plane bending
1324	1322	1323	1324	ν(C–C) In plane Isoindole
1274	1283	1296	1283	
1151	1149	1151	1152	($C_\beta - C_\beta$) Isoindole stretching
1109	1111	1112	1113	*β*(C–H) Bending in plane
1061	1063	1065	1068	*γ*(C–N) stretch in pyrole ring
952	947	948	951	γ(C–H) Out of plane deformation
882	885	887	890	
770	771	773	775	*ν*(C–N) Stretching vibration
720	732	738	732	γ(C–H) Out of plane deformation
620	623	624	625	ϕ(C–C) Macrocycle ring deformation
551	555	558	560	(C_γ–C_δ) Isoindole deformation
490	492	597	497	(C_α–C_β) Isoindole deformation

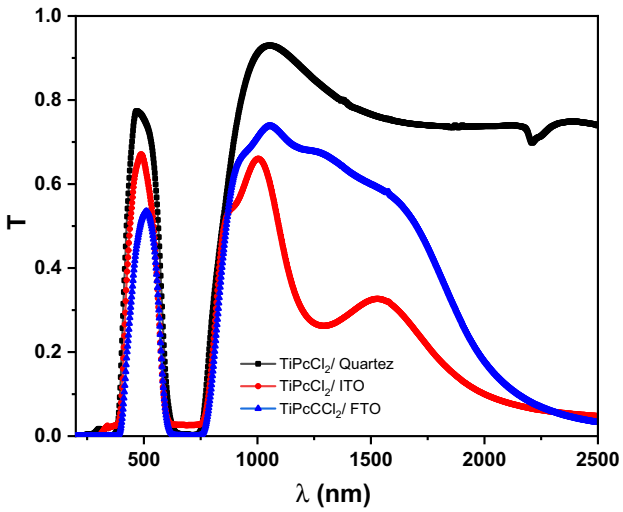

Fig. 5 The spectral distribution of reflectance for$TiPcCl_2$/quartz and $TiPcC_2$/TCSs thin films

exhibits the lowest values for E_{g1}^{Opt} and E_{g2}^{Opt}. Conversely, the $TiPcCl_2$/quartz and $TiPcCl_2$/ITO films demonstrate intermediate values, while the $TiPcCl_2$/FTO film displays the maximum value. The decline in E_{g1}^{Opt} values can be attributed to an increase in grain size and irregularity of films, resulting in the formation of defects in $TiPcCl_2$ thin films. In the context of FTO substrates, it is worth noting that the surface of $TiPcCl_2$/FTO has a rough texture when compared to microscope $TiPcCl_2$/ITO and $TiPcCl_2$/ITO, as evidenced by the FESEM photos. Also, Table 2 presents a comparison of the band gap energy values with those of other related metal MPcs compounds. Based on the data shown in the table, it can be inferred that the calculated E_{g1}^{Opt} and E_{g2}^{Opt} values for $TiPcC_{l2}$ thin films are consistent with those seen in other MPcs thin films [1, 22, 26–28, 30–35]. Table 2 illustrates a marginal disparity in the E_{g1}^{Opt} and E_{g2}^{Opt}.values observed between $TiPcCl_2$ and other MPcs, which can be attributed to the distinctive characteristics of the central metal ion present in the phthalocyanine ring and substrate nature.

The complex refractive index (N = n – jk) is a complex number that represents how the film interacts with electromagnetic waves. The real part of the refractive index, n, is connected to the phase velocity of light in the film as well as the material's electronic wave polarisation. The extinction coefficient, which is a measure of how much light is absorbed by the film, is related to the imaginary portion of the refractive index, k. The amplitude of electromagnetic waves is attenuated by a thin film when they pass through it, and this attenuation is proportional to the imaginary component of the refractive index, **k**. T(λ) and R(λ),are used to compute the optical constants (**n** and **k**) [20, 25].

$$k = \frac{\alpha\lambda}{4\pi} \tag{3}$$

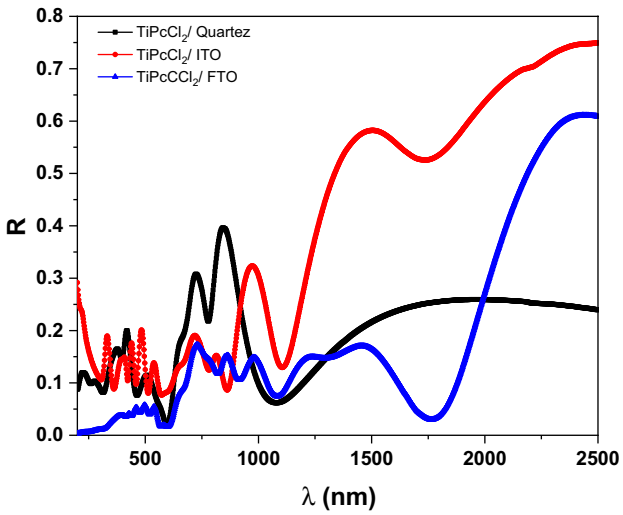

Fig. 6 The spectral distribution of transmittance for$TiPcCl_2$/quartz and $TiPcCl_2$/TCSs thin films

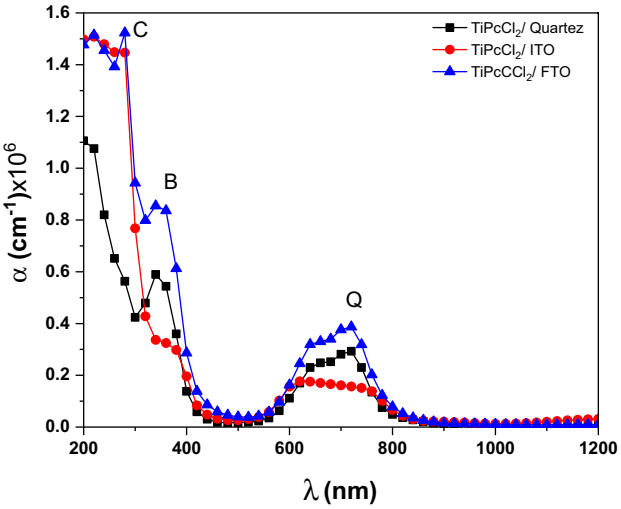

Fig. 7 Absorption coefficient forTiPcCl$_2$/quartz and TiPcCl2/ TCSs thin films

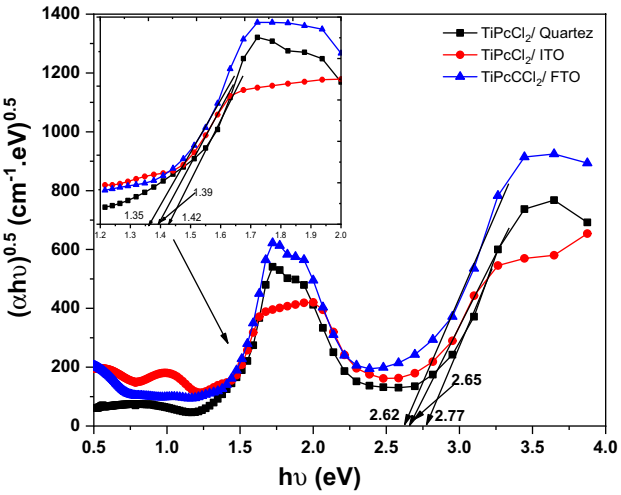

Fig. 8 Energy gap for TiPcCl$_2$/ FTO, TiPcCl$_2$/ITO and TiPcCl$_2$/ quartz thin films

Table 2 Comparison of the optical parameters of TiPcCl$_2$ with other phthalocyanine compounds

MPcs thin films	E_{g1}^{Opt}(eV)	E_{g2}^{Opt}(eV)	$\chi^{(3)}$ esu (hυ → 0)	n_2 esu (hυ → 0)	($\beta_{c\,max}$) (cm/GW)	References
TiPcCl$_2$/Quartz	1.42	2.77	1.35×10^{-12}	2.34×10^{-11}	166	Current work
TiPcCl$_2$/ITO	1.39	2.65	3.23×10^{-12}	5.11×10^{-11}	180	Current work
TiPcCl$_2$/FTO	1.35	2.59	2.12×10^{-12}	3.51×10^{-11}	204	Current work
AlPcCl/Quartz	1.36	1.91	8.21×10^{-13}	–	–	[22]
InPcCl/polyacetate	1.36	2.90	–	–	–	[1]
InPcCl/FTO	1.37	2.84			–	[28]
B-subPcCl/glass	1.90	3.44	9.60×10^{-13}	2×10^{-12}	–	[31]
B-subPcCl/polyacetate	1.91	3.19	$\sim 2.5\times10^{-12}$	$\sim 6\times10^{-11}$		[32]
B-subPcCl/FTO	1.82	3.24	–	–	–	[33]
MnPcCl/FTO	1.33	2.47	–	–	–	[26]
MnPcCl/glass	1.36	2.49	–	–	–	[30]
MnPcCl/polyacetate	1.33	2.49	–	–	–	[34]
GaPcCl/FTO	1.45	2.77	–	–	–	[27]
GaPcCl/glass	1.49	2.92	33.6×10^{-12}	41.4×10^{-11}	–	[35]

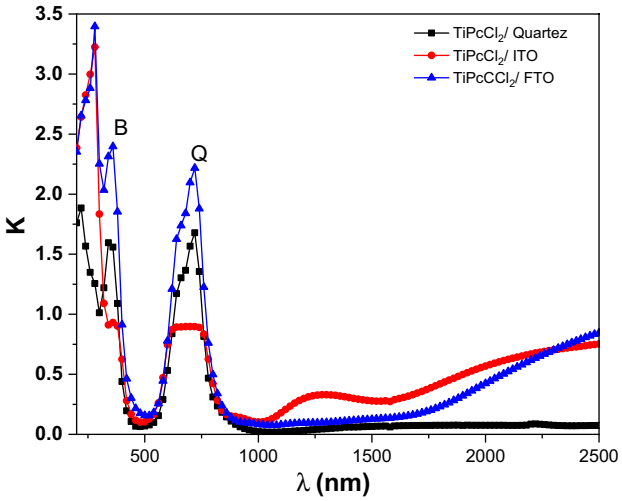

Fig. 9 Extinction index for$TiPcCl_2$/quartz and $TiPcCl_2$/TCSs thin films

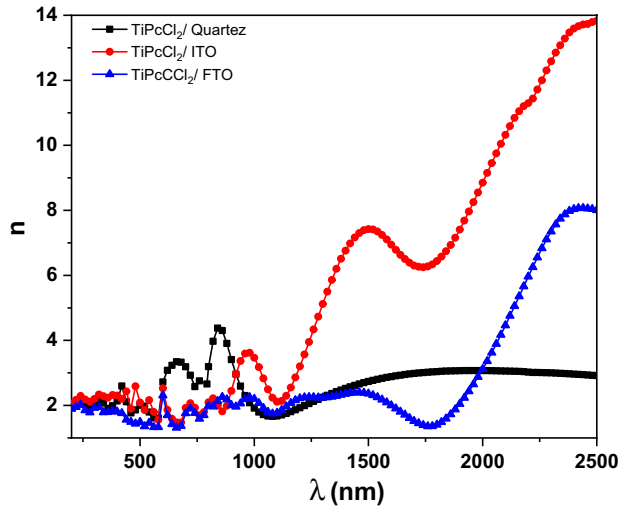

Fig. 10 Refractive index for$TiPcCl_2$/quartz and $TiPcCl_2$/TCSs thin films

$$n = \frac{1+R}{1-R} + \sqrt{\frac{4R}{(1-R)^2} - k^2} \tag{4}$$

Figure 9 depicts the variation of ***k*** with wavelength for $TiPcCl_2$/FTO, $TiPcCl_2$/ITO and $TiPcCl_2$/quartz thin films. It demonstrates that the k value for the extinction index of $TiPcCl_2$/TCSs films decreases to a minimum of about 1000 nm after that, **k** begins to increase with increasing wavelength once more; this performance is due to the influence of their free carriers in FTO and ITO substrates. The absorption of light by free carriers is referred to as free carrier absorption. The quantity of free carrier absorption increases with wavelength, which explains why the k value for the extinction index of $TiPcCl_2$/TCSs films likewise increases with wavelength. The effect of free carriers on FTO and ITO substrates on the optical characteristics of $TiPcCl_2$/TCSs films is an important element to consider when creating and using these films for applications such as solar cells and optical sensors.

The, n, is considered to be an important factor for optoelectronic devices, and the values of n for $TiPcCl_2$ thin film are calculated using Eq. (4). Figure 10 illustrates the change of n with the wavelength for $TiPcCl_2$/FTO, $TiPcCl_2$/ITO, and $TiPcCl_2$/quartz thin films. Similarly, the **k** case **n** for TiPcCl2/FTO and $TiPcCl_2$/ITO begins to increase with increasing wavelength once more; this behavior is due to the contribution of their free carriers in FTO and ITO substrates [8]. The free carriers in also interact with electromagnetic radiation, such as light, and absorb photons. The absorption of photons raises the refractive index of the substance [36]. The influence of FTO and ITO on the refractive index of thin films is determined by a variety of parameters, including the concentration of free carriers, the thickness of the

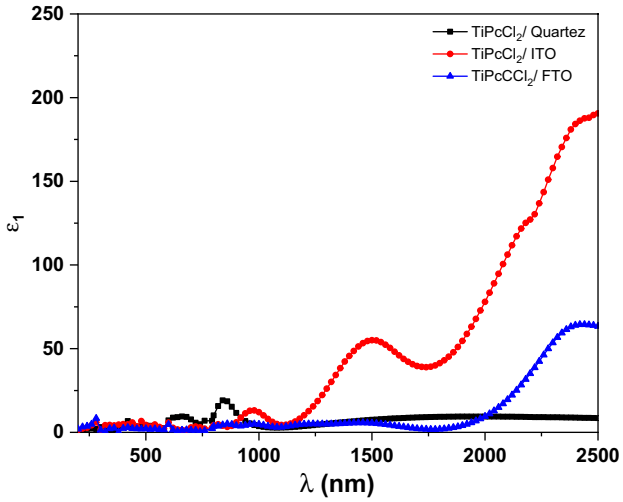

Fig. 11 Real (ε_1) part versus the wavelength for$TiPcCl_2$/quartz and TiPcCl2/TCSs thin films

film, and the wavelength of light. In general, FTO and ITO will raise the refractive index of thin films, particularly at wavelengths over the plasma wavelength.

The dielectric properties of the material affect how electromagnetic waves reflect and transmit, providing dynamic data on the electrical structure. The complicated dielectric constant components could be calculated using the optical constant [17]. The real component, denoted as $\varepsilon_1 = n^2\text{-}k^2$, corresponds to the refractive index of the material. On the other hand, the imaginary part, represented as $\varepsilon_2 = 2nk$, pertains to the energy absorption caused by interband transition and dipole dislocation.

The change in $\boldsymbol{\varepsilon_1}$ and $\boldsymbol{\varepsilon_2}$ for the $TiPcCl_2$/ITO, $TiPcCl_2$/FTO and $TiPcCl_2$/quartz thin films with wavelength dependence on refractive index values is shown in Figs. 11, 12). As a result of the contribution of TCSs free carriers, TiPcCl2/TCSs thin films exhibit higher dielectric constants at high wavelengths than $TiPcCl_2$/Quartz thin films. Free carriers can absorb photons by interacting with electromagnetic radiation such as light. Photon absorption raises the dielectric constant of the substance. Furthermore, $TiPcCl_2$/ITO thin film has higher dielectric constant values than $TiPcCl_2$/FTO thin film, particularly at long wavelengths. This is due to FTO having a lower concentration of free carriers than ITO. Quartz is a non-conductive substance having a low free carrier concentration. Because of the low concentration of free carriers, quartz has an extremely low dielectric constant regardless of the wavelength of light.

The volume energy loss function (VELF) and the surface energy loss function (SELF) are optical features of materials that characterize electron energy loss owing to interactions with the material's bulk and surface, respectively. VELF is

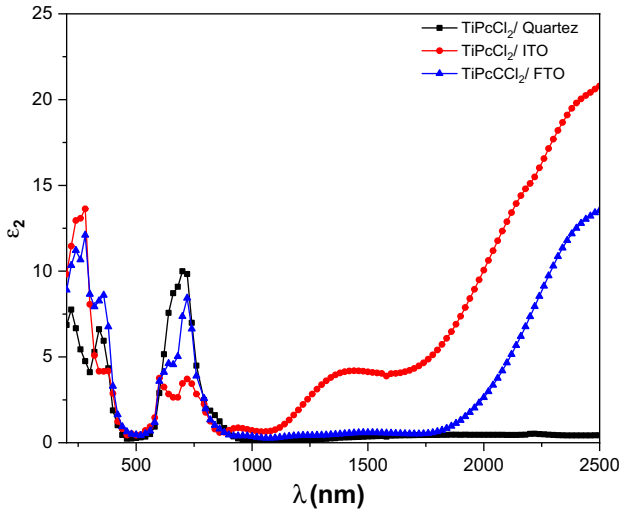

Fig. 12 The imaginary (ε_2) part versus the wavelength for$TiPcCl_2$/quartz and $TiPcCl_2$/TCSs thin films

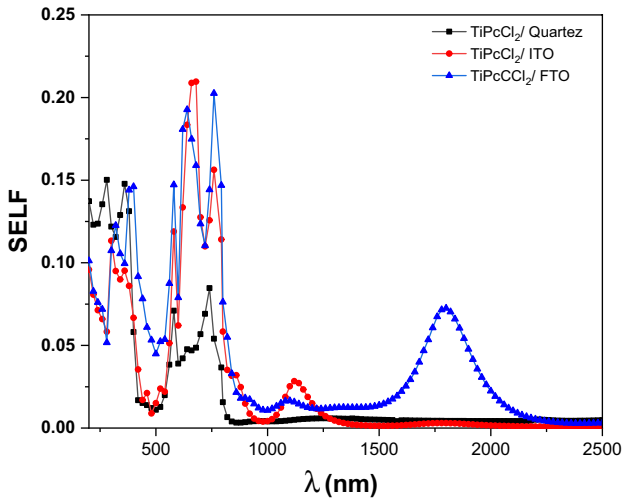

Fig. 13 The variation of SELF versus the wavelength for$TiPcCl_2$/quartz and $TiPcCl_2$/TCSs thin films

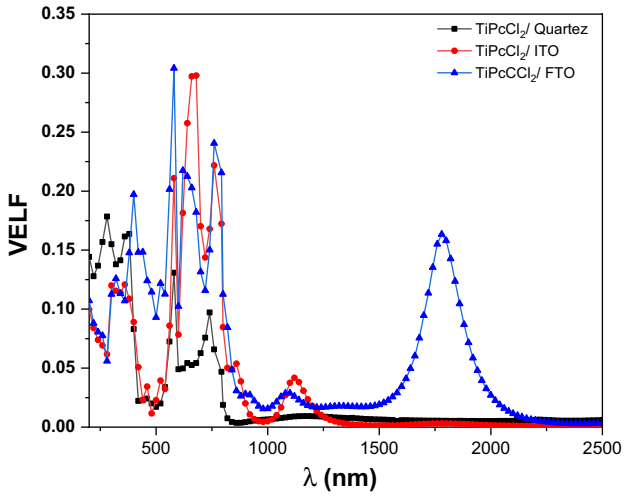

Fig. 14 The variation of VELF versus the wavelength for$TiPcCl_2$/quartz and $TiPcCl_2$/TCSs thin films

related to electronic transitions in the bulk material, while SELF is related to electronic transitions at the material's surface. The next empirical formula may be used to estimate these functions optically, which is linked to the $\boldsymbol{\varepsilon_1}$ and $\boldsymbol{\varepsilon_2}$ [10, 37]:

$$VELF = \frac{\varepsilon_2}{\left(\varepsilon_1^2 + \varepsilon_2^2\right)} \tag{5}$$

$$SELF = \frac{\varepsilon_2}{\left(\varepsilon_1 + 1\right)^2 + \varepsilon_2^2\right)} \tag{6}$$

Figures 13 and 14 explains the fluctuation of ***SELF*** and ***VELF*** relative to **λ** for $TiPcCl_2$/TCSs thin films. The obtained findings show unequivocally that the loss of energy of free charge carriers behaves about the same as that seen when it propagates over the surface. It is also clear that the volume and surface energy losses at lower wavelengths do not change considerably. This implies that energy is also attenuated by free carriers moving between the inner and outer surfaces. The high levels of VELF and SELF especially at high wavelengths are owing to a lattice mismatch between the TiPcCl2 and FTO substrates, which favors FTO over ITO. Because high-wavelength light is more readily dispersed than low-wavelength light, the impact of lattice mismatch on SELF and VELF is more severe at higher wavelengths. As a result, large levels of SELF and VELF are particularly visible at long wavelengths. By placing a buffer layer between the $TiPcCl_2$ and FTO substrates, we can mitigate the impact of lattice mismatch on SELF and VELF. The buffer layer's crystal structure should be $TiPcCl_2$ and FTO compatible. This will assist in decreasing strain

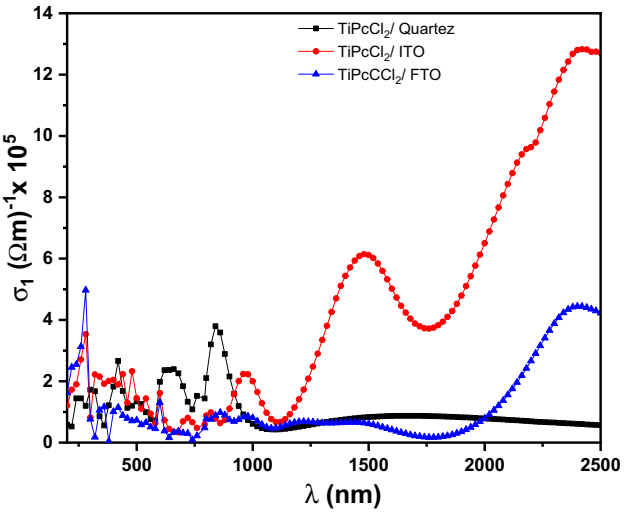

Fig. 15 The variation of real (σ_1) part versus the wavelength for$TiPcCl_2$/quartz and $TiPcCl_2$/TCSs thin films

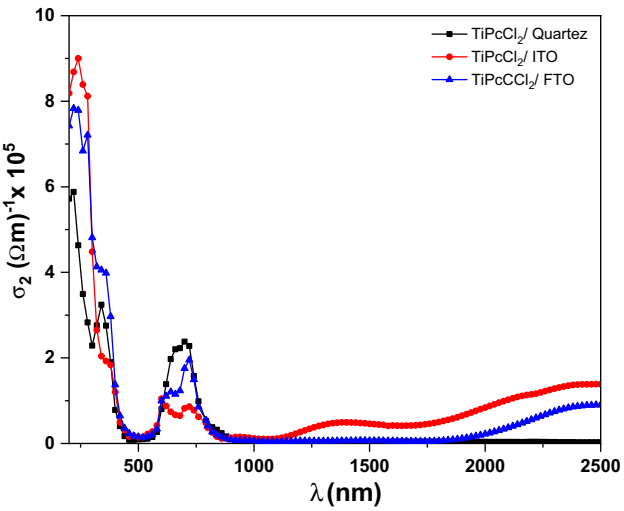

Fig. 16 The variation of imaginary (σ_2) part versus the wavelength for$TiPcCl_2$/quartz and $TiPcCl_2$/TCSs thin films

and flaws at the two materials' contact. It is feasible to lessen the impacts of lattice mismatch and increase the performance of devices using $TiPcCl_2$ and FTO substrates by following this step.

The optical response and electronic states within E_g^{opt} are studied by measuring the optical conductivity (σ_{op}). Furthermore, $\boldsymbol{\sigma_{opt}}$ is dependent on optical dielectric constants and is composed of the real $\sigma_1(\omega) = \omega\varepsilon_0\varepsilon_2$ and imaginary $\sigma_2(\omega) = \omega\varepsilon o\varepsilon_1$ parts, where ω is the angular frequency $\boldsymbol{\varepsilon_0}$ is the free space electric permittivity [14]. The variation of σ_1 and σ_2 as a function of wavelength is seen in Figs. 15 and 16. From this figure, $TiPcCl_2$/ITO is higher than $TiPcCl_2$/FTO films of σ_1 and σ_2 in infrared regain. This is likely due to a combination of factors, including the different refractive indices, surface morphologies, and free carriers concentrations of the FTO and ITO as well as the lattice mismatch between the $TiPcCl_2$ and TCSs.

3.2.1 The nonlinear parameters

The study of nonlinear optical refractive indexes in the subject of nonlinear photonics provides information on the interaction of light with these things. It is required for basic research as well as applications in materials science and photonics technology [29–31]. Based on Miller's general rule the nonlinear third-linear optical susceptibility ($\chi^{(3)}$) and nonlinear refractive index ($\boldsymbol{n_2}$) can be calculated by following formulas[38–41]:

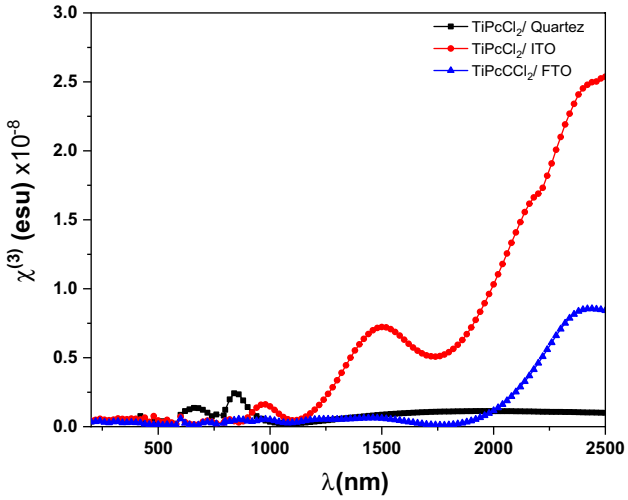

Fig. 17 The variation of $\chi^{(3)}$ versus the wavelength for for$TiPcCl_2$/quartz and $TiPcCl_2$/TCSs thin films

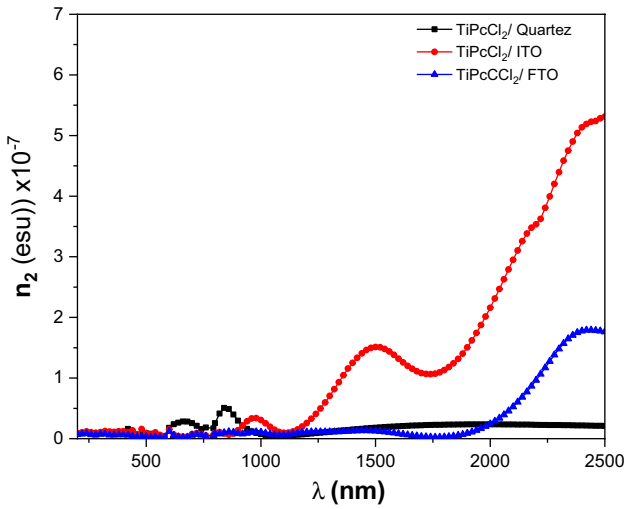

Fig. 18 The variation of $n^{(2)}$ versus the wavelength for $TiPcCl^2$/quartz and $TiPcCl_2$/TCSs thin films

$$\chi^{(3)} = 1.7 \times 10^{-10} \left(\frac{n^2 - 1}{4\pi} \right)^4 esu \tag{7}$$

$$\boldsymbol{n}_2 = \frac{12\boldsymbol{\pi}}{\boldsymbol{n}} \chi^{(3)} \, \boldsymbol{esu} \tag{8}$$

The variation of $\boldsymbol{\chi^{(3)}}$ and $\boldsymbol{n}_2$ as a function of wavelength is seen in Figs. 17 and 18. As seen in these figures $\boldsymbol{\chi^{(3)}}$ and $\boldsymbol{n}_2$ exhibit the same trend. The values of $\chi^{(3)}$ and $\boldsymbol{n}_2$ for $TiPcCl_2$/FTO and TiPcCl2/ITO are significantly greater than those for $TiPcCl_2$/Quartz. This increase in $\chi^{(3)}$ and $\boldsymbol{n}_2$ for the FTO and ITO substrates is due to the free carriers in the FTO and ITO substrates as well as the large nonlinear optical capabilities of the FTO and ITO layers, which contribute to nonlinear optical increases [11, 42, 43]. The free carriers can contribute to nonlinear optical increases through free carrier transport. When free carriers are transported through a material, they can interact with the lattice of the material and generate new photons. This process, known as free carrier bremsstrahlung, is also a nonlinear optical process. The calculation values of $\chi^{(3)}$ and, $\boldsymbol{n}_2$ at the zero-frequency (hυ = 0) using Eqs. (8) and (9) are tabled in Table 2, and are compared with those of other related metal MPcs compounds. The obtained results of the nonlinear optical values for $TiPcCl_2$/TCSs thin films suggest that $TiPcCl_2$film is an ideal material for a variety of applications that require a strong nonlinear optical response, such as optical frequency comb generation, optical parametric amplification, and optical switching.

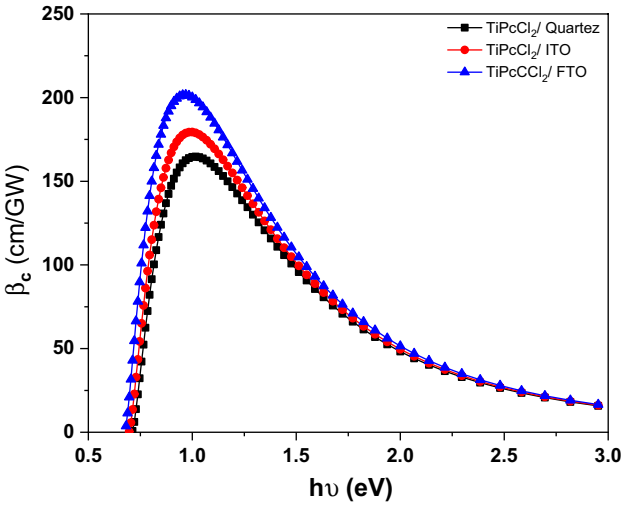

Fig. 19 The variation of βc, versus hν for $TiPcCl_2$/quartz and $TiPcCl_2$/TCSs thin films

Due to light's interaction with the semiconductor, organic thin films display a two-photon absorption (TPA) process, resulting in significant optical nonlinearity. In this TPA, two or more photons are absorbed, and the electrons are excited from the ground state to higher energy levels simultaneously, making this process largely a third-order nonlinear phenomenon. E_g^{Opt} and hν. As a result, the empirical relationship presented by Sheik-Bahae et al. provides a connection between the **βc** coefficient and E_g^{Opt} [44–46]:

$$\beta_c(\omega) = \frac{3100\sqrt{21}\left[\left(2h\nu/E_g^{Opt}\right) - 1\right]^{3/2}}{n^2 E_g^{Opt^3}\left(2h\upsilon/E_g^{Opt}\right)^5}, \text{ cm/GW} \tag{9}$$

The (βc) value upsurges with hν until it reaches a maximum value, then is reduced again (see Fig. 19 and Table 2). This is because the nonlinear absorption process is resonant, meaning that it is most efficient when the photon energy (hν) is equal to ($E_g^{Opt}/2 < h\upsilon < E_g^{Opt}$). The resonant nature of nonlinear absorption is due to the fact that the nonlinear absorption process involves two or more photons. In order for two photons to be absorbed simultaneously, they must have the same energy. This is why the nonlinear absorption coefficient is highest when the photon energy is equal to half the optical band gap of the material [44, 45]. Also, according to Fig. 19 $TiPcCl_2$/FTO thin film has the highest $\boldsymbol{\beta_{cmax}}$ this is due to the lowest E_g^{Opt} for $TiPcCl_2$/FTO thin film.

4 Conclusions

The observed changes in the structural, morphological, linear and nonlinear optical characteristics of $TiPcCl_2$ with various transparent conducting substrates are shown. XRD, FESEM and FTIR spectra verified the influence of transparent conducting substrates on the structure morphology and molecular structure of $TiPcCl_2$. The study of grain sizes from FESEM images indicates that the generated films have a nanostructured property. The drop in E_g^{Opt} values is due to increased particle size and film irregularity, which causes flaws in $TiPcCl_2$ thin films, notably on FTOsubstrate. Free carriers in FTOand ITO substrates affected dielectric constants, energy loss functions, and optical conductivity constants, notably at higher wavelengths. Another important finding of the present work is the higher values of the nonlinear optical $\chi^{(3)}$ (esu), $n^{(2)}$ (esu) and $\beta_{(c)}$ parameters for $TiPcCl_2$/TCSs than TiPcCl2/Quartz. Based on those findings, it can be concluded that $TiPcCl_2$ films exhibit very desirable characteristics for a diverse range of applications that need a robust nonlinear optical response. These applications include optical frequency comb creation, optical parametric amplification, optical switching, optical computers, and ultra-pulsed lasers.

Author contributions S. M. A: Investigation, Formal analysis, Writing-Original draft M. D: Formal analysis, Writing - Review & Editing, A. F. E: Formal analysis, Writing-Review&Editing, A. A. A: Conceptualization, Visualization, Investigation, Formal analysis, Data Curation,, Writing-Original draft, Writing - Review & Editing,

Funding Open access funding provided by The Science, Technology & Innovation Funding Authority (STDF) in cooperation with The Egyptian Knowledge Bank (EKB).

Data availability This manuscript has associated data in a data repository. [Authors' comment: All data included in this manuscript are available upon request by contacting the corresponding author].

Declarations

Competing interests The authors declare that there is no conflict of interest regarding the publication of this article.

References

1. Darwish AAA, Hamdalla TA, Al-Ghamdi SA, Alzahrani AOM, Khasim S, Yahia IS, El-Zaidia EFM. Facile deposition of non-crystalline films of indium(III) phthalocyanine chloride for flexible electronic applications. J Non-Cryst Solids. 2021;571:121043.
2. Abuelwafa AA, Yamada SI, Shibata N, Soga T. Studying linear and nonlinear optical properties of trifluoroethoxy-coated zinc phthalocyanine ((4TFEO) 4-ZnPc) thin films. Opt Mater. 2022;123:111850.
3. Choi SA, Kim K, Lee SJ, Lee H, Babajanyan A, Friedman B, Lee K. Effects of thermal preparation on copper phthalocyanine organic light emitting diodes. J Lumin. 2016;171:149.
4. Zhao W, Zou D, Sun Z, Yu Y, Yang C. Controlling spin off state by gas molecules adsorption on metal-phthalocyanine molecular junctions and its possibility of gas sensor. Phys Lett A. 2018;382:2666.
5. Urbani M, Ragoussi M-E, Nazeeruddin MK, Torres T. Phthalocyanines for dye-sensitized solar cells. Coord Chem Rev. 2019;381:1.
6. Melville OA, Lessard BH, Bender TP. Phthalocyanine-based organic thin-film transistors: a review of recent advances. ACS Appl Mater Interfaces. 2015;7:13105.
7. Cherian RC, Menon C. Preparation and characterization of thermally evaporated titanium phthalocyanine dichloride thin flms. J Phys Chem Solids. 2008;69:2858.
8. Al-Ghamdi SA, Hamdalla TA, Darwish AAA, Alzahrani AOM, El-Zaidia EFM, Alamrani NA, Elblbesy MA, Yahia IS. Preparation, Raman spectroscopy, surface morphology and optical properties of $TiPcCl_2$ nanostructured films: thickness effect. Opt Quantum Electron. 2021;53:514.
9. Vergara MES, Heredia LFV, Hamui L. Influence of the coordinated ligand on the optical and electrical properties in titanium phthalocyanine-based active ilms for photovoltaics. Materials. 2023;16:551.
10. Elnobi S, Abd El-sadek MS, Yahia IS, Zahran HY, Abuelwafa AA. Correlation between structural, morphological, and optical properties of spin-coated poly(2,5-di(hexyloxy) cyanoterephthalylidene) (CN-PPV) thin films. J Mater Sci Mater Electron. 2022;33:22092.
11. Abuelwafa AA, Abd El-sadek MS, Elnobi S, Soga T. Effect of transparent conducting substrates on the structure and optical properties of Tin(II) oxide (SnO) thin films: comparative study. Ceram Int. 2021;47:13510.
12. Lee J-B, Lee M-H, Park C-K, Park J-S. Effects of lattice mismatches in ZnO/substrate structures on the orientations of ZnO films and characteristics of SAW devices. Thin Solid Films. 2004;447–448:296.
13. Ribut SH, Abdulla CAC, Yusoff MZM. Investigations of structural and optical properties of zinc oxide thin films growth on various substrates. Results Phys. 2019;13:102146.
14. Rodriguez RC, Oliva AI, Sosa V, Briones FC, Peña JL. Effect of indium tin oxide substrate roughness on the morphology, structural and optical properties of CdS thin films. Appl Surf Sci. 2000;161:340.
15. Hasani E, Kamalian M, Arashti MG, Habashi LB. Effect of substrate properties on nanostructure and optical properties of CdTe thin films. J Electron Mater. 2019;48:4283.
16. Krataithong C, Srichai K, Wongrat E, Tubtimtae A. Comparative study on the influence of transparent glass substrates for antimony telluride thin films via structural and optical properties. J Sci Adv Mater Dev. 2022;7:100449.
17. Abuelwafa AA, AbdEl-sadek MS, Yahia IS. Linear and nonlinear optical properties of nano-spherical perylenetetracarboxylic dianhydride/ITO as a new optical system. Opt Laser Technol. 2018;108:241.
18. Abuelwafa AA, Alsoghier HM, Elnobi S, Dongol M, Soga T. Quantum computational, linear and non-linear optical properties of spin-coated nickel(II)-tetraphenylporphyrin/FTO thin films. Optik. 2021;234:166618.
19. Ebied MS, Dongol M, Ibrahim M, Nassary M, Elnobi S, Abuelwafa AA. Structural and optical properties of nanocrystalline 3-(2-benzothiazolyl)-7-(diethylamino) coumarin (C6) thin films for optoelectronic application. J Electron Mater. 2022;51:5770.
20. Abuelwafa AA, El-Denglawey A, Dongol M, El-Nahass MM, Soga T. Influence of annealing temperature on structural and optical properties of nanocrystalline platinum octaethylporphyrin (PtOEP) thin films. Opt Mater. 2015;49:271.

21. Akgul FA, Akgul G, Yildirim N, Unalan HE, Turan R. Influence of thermal annealing on microstructural, morphological, optical properties and surface electronic structure of copper oxide thin films. Mater Chem Phys. 2014;147:987.
22. El-Nahass MM, Khalif BA, Soliman IM. Gamma radiation-induced changes on the structural and optical properties of aluminum phthalocyanine chloride thin films. Opt Mater. 2015;46:115.
23. Tackley DR, Dent G, Smith WE. IR and Raman assignments for zinc phthalocyanine from DTF calculations. Phys Chem Chem Phys. 2000;2:3949.
24. Milev AS, Tran N, Kannangara GSK, Wilson MA, Avramov I. Polymorphic transformation of iron-phthalocyanine and the effect on carbon nanotube synthesis. J Phys Chem C. 2008;112:5339.
25. Abuelwafa AA, Matiur RMD, Putri AA, Soga T. Synthesis, structure, and optical properties of the nanocrystalline bismuth oxyiodide (BiOI) for optoelectronic application. Opt Mater. 2020;109:110413.
26. Darwish AAA, Helali S, Qashou SI, Yahia IS, El-Zaidia EFM. Studying the surface morphology, linear and nonlinear optical properties of manganese(III) phthalocyanine chloride/FTO films. Phys B Phys Condens Matter. 2021;622:413355.
27. Darwish AAA, Hamdalla TA, El-Zaidia EFM, Hanafy TA, Issa SAM, Yahia IS. Thin films of nanostructured gallium(III) chloride phthalocyanine deposited on FTO: structural characterization, optical properties, and laser optical limiting. Phys B Phys Condens Matter. 2020;593:412321.
28. Alghamdi SA, Darwish AAA, Yahia IS, El-Zaidia EFM. Structural characterization and optical properties of nanostructured indium(III) phthalocyanine chloride/FTO thin films for photoelectric applications. Optik. 2021;239:166780.
29. Alfadhli S, Darwish AAA, Soliman S, El-Zaidia EFM, Yahia IS, Laariedh F, Alatawi A, Bahamran A, Alatawi NM, Hamdalla TA. Structural characterizations and photoelectric performance of non-crystalline boron subphthalocyanine chloride films/FTO for photodiode applications. J Non-Cryst Solids. 2023;601:122044.
30. El-Zaidia EFM. Studies structure, surface morphology, linear and nonlinear optical properties of nanocrystalline thin films of manganese(III) phthalocyanine chloride for photodetectors application. Sens Actuat A. 2021;330:112828.
31. El-Zaidia EFM, Bousbih R, Darwish AAA, Qashou SI, Mohammedsaleh ZM, Bassfar Z, Yahia IS, Abu-Samaha FS. Effect of film thickness on structural, electrical and optical properties of amorphous boron subphthalocyanine chloride thin film. Opt Mater. 2023;138:113691.
32. El-Zaidia EFM, Hamdalla TA, Ali HAM, Alghamdi N, Alfadhli S, Yahia IS, Soliman S, Bani-Atta SA, Darwish AAA. Boron sub-phthalocyanine chloride deposited on PA substrate towards flexible optoelectronic devices: structural, optical, and electrical characterization. Physica B. 2023;668:415250.
33. Alfadhli S, Darwish AAA, Soliman S, El-Zaidia EFM, Yahia IS, Laariedh F, Alatawi A, Bahamran A, Alatawi NM, Hamdalla TA. Structural characterizations and photoelectric performance of non-crystalline boron subphthalocyanine chloride films/FTO for photodiode applications. J Non-Crystal Solids. 2023;601:122044.
34. Darwish AAA, Ali HAM, El-Zaidia EFM, Alfadhli S, El-Bashir BO, Alatawi RAS, Eisa AAA, Yahia IS. Linear and nonlinear optical characteristics of manganese phthalocyanine chloride/polyacetate sheet: towards flexible optoelectronic devices. Opt Mater. 2021;114:110988.
35. El-Zaidia EFM, Qashou SI, Darwish AAA, Yahia IS. Thermally evaporated of homogeneous nanostructured gallium-phthalocyanine-chloride films: optical spectroscopy. Opt Mater. 2020;109:110407.
36. Kalanoor BS, Gouda L, Gottesman R, Tirosh S, Haltzi E, Zaban A, Tischler YR. Third-order optical nonlinearities in organometallic methylammonium lead iodide perovskite thin films. ACS Photon. 2016;3:361.
37. Wasly HS, El-Sadek A, Elnobi S, Abuelwafa AA. Morphological, structural, and optical properties of flexible tin oxide(II) thin film via thermal evaporation technique. Eur Phys J Plus. 2022;137:164.
38. Alsoghier HM, Selim MA, Salman HMA, Rageh HM, Santos MA, Ibrahim SA, Dongol M, Soga T, Abuelwafa AA. NMR spectroscopic, linear and non-linear optical properties of1,3-benzothiazol-2-yl-(phenylhydrazono)acetonitrile (BTPA) azo dye. J Mol Struct. 2019;1179:315.
39. Zahran HY, Iqbal J, Yahia IS. Optical constants and nonlinear calculations of fluorescein/FTO thin film optical system. Phys B Condens Matter. 2016;500:98.
40. Gami F, Guizani I, Sebak MA, Abuelwafa AA, Mostafa MM. Investigation of structural, optical and electrical properties of PCBM/ZnOEP thin films. Opt Mater. 2022;134:113093.
41. Tichá H, Tichý L. Semiempirical relation between non-linear susceptibility (refractive index), linear refractive index and optical gap and its application to amorphous chalcogenides. J Optoelectron Adv Mater. 2002;4:381.
42. Wu Z, Wang J, Yang H. Ye, Large optical nonlinearity of ITO/Ag/ITO sandwiches based on Z-scan measurement. Opt Lett. 2019;44:2490.
43. Guo P, Schaller RD, Ocola LE, Diroll BT, Ketterson JB, Chang RPH. Large optical nonlinearity of ITO nanorods for sub-picosecond all-optical modulation of the full-visible spectrum. Nat Commun. 2016;7:12892.
44. Sheik-Bahae M, Hagan DJ, Van Stryland EW. Dispersion and band-gap scaling of the electronic Kerr effect in solids associated with two-photon absorption. Phys Rev Lett. 1990;65:96.
45. Sheik-Bahae M, Hutchings DC, Hagan DJ, Stryland EWV. Dispersion of bound electron nonlinear refraction in solids. IEEE J Quantum Electron. 1991;27:1296.
46. Stenzel O, Wilbrandt S, Mühlig C, Schröder S. Linear and nonlinear absorption of titanium dioxide films produced by plasma ion-assisted electron beam evaporation: modeling and experiments. Coatings. 2020;10:59.